朱红伟，程佑法，李婷，等. 水热法合成的一种新型祖母绿宝石学及光谱学特征[J]. 岩矿测试，2023，42(2)：307-316. doi：10.15898/j.cnki.11-2131/td.202203290067.

ZHU Hongwei，CHENG Youfa，LI Ting，et al. Gemological and Spectral Characteristics of a New Type of Emerald Synthesized by the Hydrothermal Method[J]. Rock and Mineral Analysis，2023，42(2)：307-316. doi：10.15898/j.cnki.11-2131/td.202203290067.

水热法合成的一种新型祖母绿宝石学及光谱学特征

朱红伟[1,2]，程佑法[1,2]，李婷[1,2]，马霄[1,2]，丁秀云[1,2]，范春丽[1,2]，赵潇雪[1,2]，陈淑祥[3]，胡建华[4]
(1. 山东省计量科学研究院，山东 济南 250014；
2. 国家黄金钻石制品质量检验检测中心，山东 济南 250014；
3. 齐鲁工业大学(山东省科学院)，山东 济南 250353；
4. 深圳市深智检测技术有限公司，广东 深圳 518020)

摘要： 水热法是合成祖母绿的常用方法之一，使用该方法合成的祖母绿具有典型“水波纹”状纹理，呈现锯齿状平行排列，且其红外透射吸收光谱在 2300~3100cm^{-1} 的特征峰是主要鉴定特征。但目前市场上新出现的水热法合成的一种祖母绿不具有上述典型特征。为探究这种水热法合成的祖母绿的宝石学和光谱学特征，本文采用常规宝石学仪器宝石显微镜、折射仪等及红外吸收光谱仪、紫外可见光谱仪、能量色散 X 射线荧光光谱仪(EDXRF)对其鉴定特征进行研究分析。结果表明：测试样品的折射率为 1.571~1.588，双折射率为 0.007~0.009，相对密度为 2.56~2.78，多色性明显，这些特征与天然祖母绿相似，红外吸收光谱特征与天然祖母绿基本一致。在宝石显微镜下，从特定角度观察可见疑似水热法合成祖母绿的“水波纹”状纹理，呈平行状，但不是典型的锯齿状平行排列，属于疑惑样品。红外透射吸收光谱具有Ⅰ型水和Ⅱ型水的尖锐吸收峰，在 2300~3100cm^{-1} 范围内的吸收相对较弱，不具有诊断意义；紫外可见光谱分析表明 Fe^{2+} 离子引起的 810~850nm 吸收宽带不明显，但 810~850nm 范围内的特征吸收带是天然祖母绿的重要鉴定特征。能量色散 X 射线荧光光谱仪(EDXRF)分析显示样品含有异常高的 Ni 元素，其 Ni 元素的 Kα 峰强度远大于 Cr 元素的 Kα 峰强度(2 倍以上)，但研究表明世界各地的天然祖母绿中几乎不含 Ni 元素，或 Ni 元素含量低于 Cr 元素含量的 2‰。经综合分析这种水热法合成的新型祖母绿的关键鉴定特征是，在结合紫外可见吸收光谱特征即 Fe^{2+} 离子引起的 810~850nm 吸收宽带不明显的同时，重点关注 EDXRF 测试结果，其 Ni 元素的 Kα 峰强度显著大于 Cr 元素的 Kα 峰强度。

关键词： 祖母绿；水热法；红外光谱法；紫外可见光谱法；X 射线荧光光谱法；鉴定特征

要点：

(1) 采用常规宝石学仪器和红外光谱分析的检测方法不能确定该类新型合成祖母绿的成因。

(2) 该类新型合成祖母绿的关键检测特征是 EDXRF 分析的 Ni 元素的峰强度远远大于 Cr 峰强度，并且紫外可见光谱中 810~850nm 吸收宽带不明显。

(3) 该类新型合成祖母绿的准确鉴定需要多种方法的综合分析。

中图分类号： O657.33；O657.32 **文献标识码：** A

收稿日期： 2022-03-29；**修回日期：** 2022-07-20；**接受日期：** 2022-10-01

基金项目： 山东省重点研发计划项目“山东长清木鱼石产业质量安全关键技术与标准研究”(2017GSF220015)

作者简介： 朱红伟，高级工程师，从事珠宝玉石及贵金属检测。E-mail：red8761@163.com。

祖母绿因其艳丽的颜色而受到人们的喜爱，被尊崇为世界四大宝石之一，特别最近几年随着彩色宝石市场的成熟与发展，人们对祖母绿越来越追崇。由于祖母绿价值昂贵，多种合成和优化处理方法层出不穷。珠宝检测中常用的常规宝石学测试和红外吸收光谱法难以准确鉴别。

前人对祖母绿以及合成祖母绿作了比较细致的研究，总结了红外吸收光谱、紫外可见光谱、LA-ICP-MS 等鉴定方法和鉴定特征。石国华[1]重点研究了桂林水热法合成祖母绿的红外光谱特征及内含物特征，指明红外吸收光谱在 2300~3100cm^{-1} 范围的特征吸收峰是其主要的鉴定特征。杨卓[2]研究了云南祖母绿与其他产地祖母绿的成分特征，均未发现天然祖母绿中含有 Ni 元素，但均含有 Cr 元素。孙主等[3]详细阐述了俄罗斯水热法合成祖母绿的红外光谱特征及其成分特征，认为红外吸收光谱是其重要的鉴定手段。申柯娅[4]认为红外吸收光谱和内含物特征是鉴定天然祖母绿、水热法合成祖母绿、助溶剂法合成祖母绿的重要证据。邵慧娟等[5]认为红外透射光谱是鉴定合成祖母绿的重要依据。Karamplelas 等[6]研究了包括阿富汗、巴西、哥伦比亚、埃塞俄比亚、马达加斯加、俄罗斯、赞比亚、津巴布韦等不同产地祖母绿的成分特征，利用激光剥蚀电感耦合等离子体质谱仪（LA-ICP-MS）测试证明了这些天然祖母绿均含有 Cr 元素，Ni 元素含量极低或低于检出限。Huong 等[7]利用拉曼光谱法分析了天然祖母绿与合成祖母绿的光谱特征，认为拉曼光谱是鉴定祖母绿的重要手段。前人的结果研究均将红外吸收光谱作为鉴定天然祖母绿与合成祖母绿的重要依据。水热法合成祖母绿放大观察时常见典型的水波纹状生长纹理，呈平行锯齿状分布，是其鉴定的要点之一，此外红外吸收光谱中 2300~3100cm^{-1} 范围内出现的 Cl$^-$ 吸收峰是区分天然祖母绿和水热法合成祖母绿的重要证据。

本文作者课题组在日常检测中遇到一种新型合成祖母绿样品，其基本宝石学特征、红外吸收光谱特征等与天然祖母绿极为相似，用红外吸收光谱分析并不能获得其成因的佐证证据。基于此，通过使用紫外可见光谱、能量色散 X 射线荧光光谱仪（EDXRF）等多种谱学手段，综合开展了测试样品的宝石学和光谱学特征研究，最终确定该测试样品为水热法合成的一种新型祖母绿。

1 样品基本特征

样品为一批绿色刻面型戒面，带有蓝色色调的绿色，玻璃光泽，透明，单粒质量在 0.17~0.56g 之间，肉眼观察内部较为洁净，品质很好。

2 样品常规宝石学鉴定方法及特征分析

采用常规宝石学检测方法测试样品。滤色镜下呈浅粉红色；正交偏光镜下可见似明似暗现象，为各向异性宝石；质量、尺寸、折射率、相对密度、多色性等基本特征见表 1。在宝石显微镜下观察样品，采用顶光源观察冠部，样品表面抛光良好，棱线平直（图 1a）。采用底光源透射光暗域法从台面观察内部具有平行生长纹理（图 1b），黑色点状包体（图 1c）。采用顶光源从亭部观察，某个合适角度可见似水热法合成祖母绿特征的“水波纹”状纹理（图 1d），但不像前人研究结果那么典型，呈现为平行锯齿状纹理特征。

通过常规宝石学特征测试，该批样品确认为“祖母绿类”，但不能确定是否为天然祖母绿，其疑似“水波纹”状纹理应引起警觉。通常水热法合成祖母绿特有的“水波纹”特征非常典型，呈现锯齿状平行排列，但该样品这种特征不典型，只是局部可见。测试样品中的黑色点状包裹体，边界不清晰，形状不规则。在天然祖母绿中黑色包裹体常为磁铁矿或碧玺，边界清晰，磁铁矿呈较为规则的六边形，而碧玺的横切面具有典型的似三角形结构。

表 1 样品的规格、折射率、相对密度、多色性特征

Table 1 Size, refractive index, relative density, and polychromatic characteristics of the samples

样品编号	质量(g)	尺寸(mm)	折射率	双折射率	相对密度	多色性特征
1	0.5583	8.47×8.02×5.83	1.573~1.580	0.007	2.56	明显：蓝绿色/绿色
2	0.1748	7.01×4.98×3.53	1.572~1.581	0.009	2.72	明显：蓝绿色/绿色
3	0.1803	6.99×4.98×3.50	1.578~1.585	0.007	2.69	明显：蓝绿色/绿色
4	0.2067	7.95×5.94×3.71	1.579~1.588	0.009	2.75	明显：蓝绿色/绿色
5	0.2015	7.98×5.98×3.66	1.571~1.579	0.008	2.78	明显：蓝绿色/绿色

(a) 表面切磨良好，棱线平直(15X)　　(b) 从台面观察可见平直生长纹理(15X)

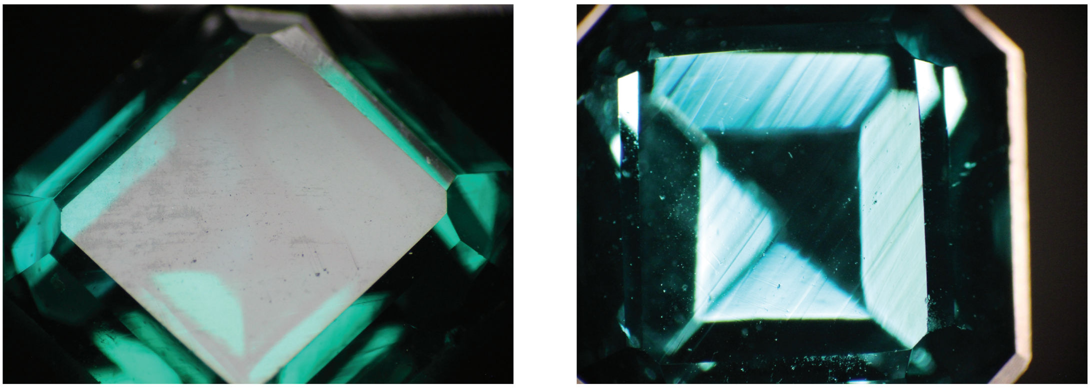

(c) 内部具有黑色点状包体(30X)　　(d) 亭部某个角度可见疑似“水波纹”生长纹理(15X)

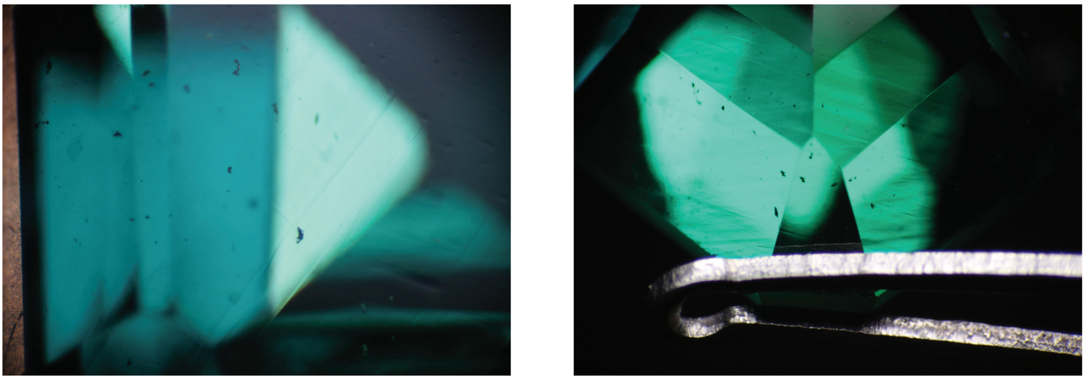

图 1　样品放大观察特征

Fig. 1　Magnification characteristics of the samples. (a) The surface was well cut , the edges were straight (15X); (b) Straight growing texture could be observed from the mesa observation (15X); (c) There were black dotted inclusions inside (30X); (d) Suspected water ripple growth texture could be seen from an angle of the pavilion (15X).

3　样品光谱鉴定方法及特征分析

3.1　红外光谱鉴定方法及特征分析

3.1.1　测试条件

采用德国 BRUKER TENSOR 27 型傅里叶变换红外光谱仪,利用漫反射附件和直接透射法,测试条件为:室温 27℃,相对湿度 35%,分辨率为 8cm^{-1},扫描次数为 64 次,测量范围为 400 ~ 6000cm^{-1}。测试样品的反射光谱和透射光谱。

3.1.2　测试结果及光谱特征分析

样品的红外反射光谱见图 2a,具有 1242、1219、1022、968、810、741、687、594、528、490、459cm^{-1} 特征峰,其中 1242、1219、1022、968、810、741、687cm^{-1} 特征峰为 Si—O—Si 和 O—Si—O 的伸缩振动所致,594、528、490、459cm^{-1} 特征峰为 Si—O 弯曲振动和 M—O 的振动所致[8]。样品的红外反射光谱特征与绿柱石的红外光谱特征一致[9],但是指纹区的红外光谱特征不能反映样品是否为天然与合成。

样品的红外透射光谱见图 2b,显示 5445、5273、5109、4874、4800、4650、4547、3321、3222、3027、2953、2928、2431cm^{-1} 特征峰。

根据张嘉麟等[10]研究,在绿柱石中水只能存在于通道中,即环间通道位置,且存在Ⅰ、Ⅱ两种类型。Ⅰ型水:水分子的对称轴垂直于结构中的 C 轴,即 H—H 的方向平行于 C 轴排列。Ⅱ型水:水分子对称轴平行于结构的 C 轴,H—H 方向垂直于 C 轴排列。Ⅱ型水的存在与通道中碱金属有关,当通道中有碱金属存在时,与水毗邻的碱金属离子产生的电场使水分子相对于Ⅰ型水旋转了 90°,并且使水伸缩振动和弯曲振动的频率略有升高,Si—O 环之间的键力也比Ⅰ型水强。5273cm^{-1} 为Ⅱ型水吸收所致,5445cm^{-1} 和 5109cm^{-1} 为Ⅰ型水吸收所致。石国华[1]利用红外吸收光谱研究了不同产地的祖母绿水的红外特征峰,经过对比发现天然祖母绿Ⅱ型水的红外特征峰一般较为宽大,且Ⅰ型水的吸收峰较弱。

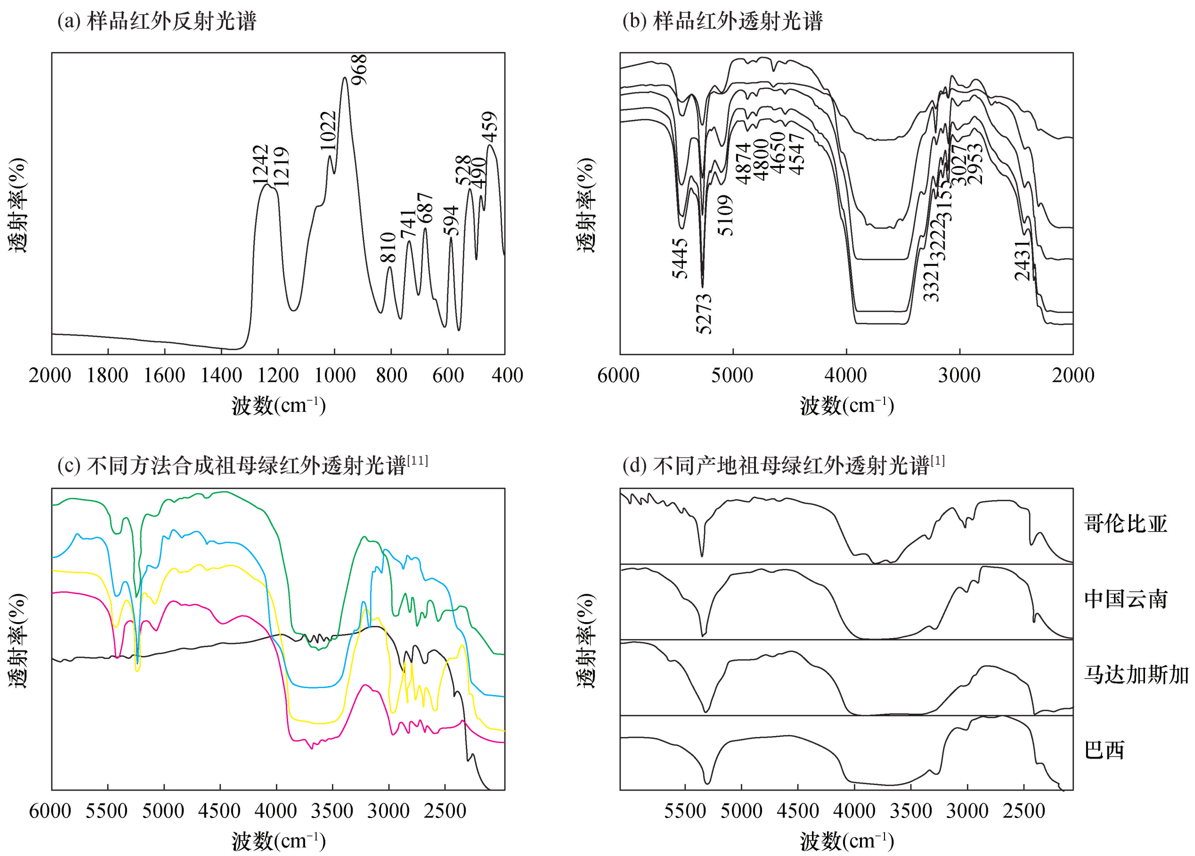

(a) 样品红外反射光谱

(b) 样品红外透射光谱

(c) 不同方法合成祖母绿红外透射光谱[11]

(d) 不同产地祖母绿红外透射光谱[1]

图 2　天然祖母绿和合成祖母绿红外光谱谱图

Fig. 2　FTIR spectra of natural emeralds and synthetic emeralds. (a) Infrared reflectance spectra of the sample; (b) Infrared transmission spectra of the sample; (c) Infrared transmission spectra of emerald synthesized by different methods[11]; (d) Infrared transmission spectra of emeralds from different origins[1].

通过对比发现，此样品的Ⅱ型水吸收峰 5273cm^{-1} 比较尖锐，并且Ⅰ型水吸收峰 5445cm^{-1} 和 5109cm^{-1} 相对较强。对比前人研究结果，天然祖母绿与水热法合成祖母绿的水的吸收峰形状，测试样品的红外吸收光谱特征与天然祖母绿存在一定差异，但不能从红外吸收光谱获得诊断性的直接证据。

2300～3100cm^{-1} 范围内红外峰为 Cl$^-$离子吸收所致，根据石国华[1]、张蓓莉[11]等学者的研究结果，“金伯利”、俄罗斯、桂林及林德水热法合成祖母绿（图 2c）在此波数范围内的吸收强度明显强于天然祖母绿。但是通过分析本文涉及样品的红外吸收光谱，在 2300～3100cm^{-1} 范围内吸收相对较弱，与哥伦比亚、中国云南、马达加斯加、巴西的天然祖母绿的红外吸收光谱特征（图 2d）更为相似，与前人研究水热法合成祖母绿的红外吸收光谱结果明显不同。

通过以上红外光谱的分析，难以确定测试样品的成因属性，需要进一步通过测试确认。传统的水热法合成祖母绿与天然祖母绿的红外吸收光谱有明显的差别，红外吸收光谱特征是鉴定祖母绿成因的重要证据，但本文的测试样品从红外吸收光谱分析难以获得最终的准确结论，因此我们称之为“新型”品种。

3.2　紫外可见光谱鉴定方法及特征分析

3.2.1　测试条件

采用广州标旗光电科技发展股份有限公司的 GEM-3000（Ⅲ）型紫外可见光光谱仪，测试条件为：积分时间 50s，平均次数 30，平滑度为 2，测试范围为 225～1000nm，室温 27℃，相对湿度 45%。

3.2.2　测试结果及光谱特征分析

样品的紫外可见光谱特征如图 3 所示，350nm 以下的吸收峰为祖母绿中 Fe^{2+}－O^{2-} 荷移带所致，429nm 吸收峰为 Cr^{3+} 离子所致，550～650nm 的宽大吸收带主要是由 Cr^{3+} 离子所致，683nm 吸收峰为 Cr^{3+}离子所致，956nm 尖锐的吸收峰是由水的吸收所致，850nm 附近的宽吸收峰应该是 Fe^{2+}吸收所致，这是在以往水热法合成祖母绿中极少出现的。个别样品中的 800nm 吸收峰起因未能分析。

Cr^{3+} 和 Fe^{3+} 替代 Al^{3+} 的联合作用使得祖母绿呈现绿色。但是在天然祖母绿中,根据 Wood 等[12]的研究,天然祖母绿的紫外可见光谱具有 Fe^{2+} 吸收所致的 830nm 附近吸收带,对于鉴定天然祖母绿具有重要意义。Qin 等[13]经紫外可见光谱分析证明印度祖母绿具有 Fe^{2+} 所致的 850nm 吸收峰。Saeseaw 等[14]利用紫外可见光谱分析中国、阿富汗、哥伦比亚、巴西、埃塞尔比、俄罗斯、马达加斯加、赞比亚祖母绿具有明显的 Fe^{2+} 所致的 810nm 吸收宽带,但是在哥伦比亚和阿富汗低铁祖母绿样品中 Fe^{2+} 所致的 810nm 吸收不明显。Guo 等[15]利用紫外可见光谱分析证明巴基斯坦祖母绿具有强而宽的 Fe^{2+} 所致的 850nm 吸收带。Krzemnicki 等[16]研究表明阿富汗潘杰希尔祖母绿的紫外可见光谱分析具有 Fe^{2+} 所致的 830nm 吸收宽带。Bai 等[17]研究表明中国云南祖母绿 Fe^{2+} 所致的吸收带位于 837nm。乔鑫等[18]研究表明根据红外光谱可对贫碱低类质同象替换成因的 I 型水祖母绿进行初步识别。由此可见在天然祖母绿中 Fe^{2+} 所致的紫外可见光谱吸收峰在 810 ~ 850nm 范围内,并且只有极少数天然祖母绿中 Fe^{2+} 所致的吸收带不明显。测试样品的紫外可见光谱在 810~850nm 范围内的吸收带不明显或微弱,个别样品 850nm 吸收峰较为明显。因此,通过紫外可见光谱分析可能是合成品,但不能给出明确结论。

3.3 能量色散 X 射线荧光光谱鉴定方法及特征分析

3.3.1 测试条件

采用 EDX 3000 Plus X 射线荧光光谱仪(江苏天瑞仪器股份有限公司),测试条件为:室温,管压 40kV,管流 300mA,铝质薄滤光片,准直器 4mm,测量时间 30s。

3.3.2 测试结果及光谱特征分析

测试结果表明,样品具有 Fe、Ni、Cr 元素(图 4),由于非真空条件测试,轻元素未能显示。杨卓[2]利用 LA-ICP-MS 精确测量了巴西、哥伦比亚、埃及、印度、南非、津巴布韦、加拿大等不同产地祖母绿中的主要微量元素,研究结果表明,天然祖母绿中主要微量元素有 Fe、V、Cr、Mg、Na、Cs 等,但 Ni 含量很低,远远低于 Cr 元素;Bai 等[17]利用 LA-ICP-MS 分析云南祖母绿中的微量元素 Cr 含量为 58~177μg/g,未检出 Ni 元素。Karampelas 等[6]研究阿富汗、巴西、哥伦比亚、埃塞俄比亚、马达加斯加、俄罗斯、赞比亚和津巴布韦宝石级祖母绿化学元素特征,利用 LA-ICP-MS 分析显示 Ni 元素未检出。Pignatelli 等[19]分析哥伦比亚达碧兹型祖母绿成分显示,样品中未检测出 Ni 元素。Lum 等[20]对祖母绿的地球化学特征进行分析,电子探针结果表明南非、阿富汗、澳大利亚、哥伦比亚、埃及、马达加斯达、赞比亚、津巴布韦、坦桑尼亚祖母绿中未检测到 Ni 元素。Qin 等[13]利用 LA-ICP-MS 分析云南祖母绿化学成分中未检测出 Ni 元素。任伟等[21]和代鸿章等[22]利用电子探针分别分析了中国新疆祖母绿和陕西祖母绿,均未检测出 Ni 元素。由此可见天然祖母绿中 Cr、Fe 元素同时存在,但 Ni 元素几乎不存在。

根据前人研究结果,天然祖母绿中几乎不含 Ni 元素,即使检出 Ni 元素其含量也低于 Cr 元素(低于幅度 2‰)[2,16]。本文采用能量色散 X 射线荧光光谱仪,未进行定量化分析。采用的仪器是经过黄金标准样品标定的,元素相对峰强度具有重要意义,通

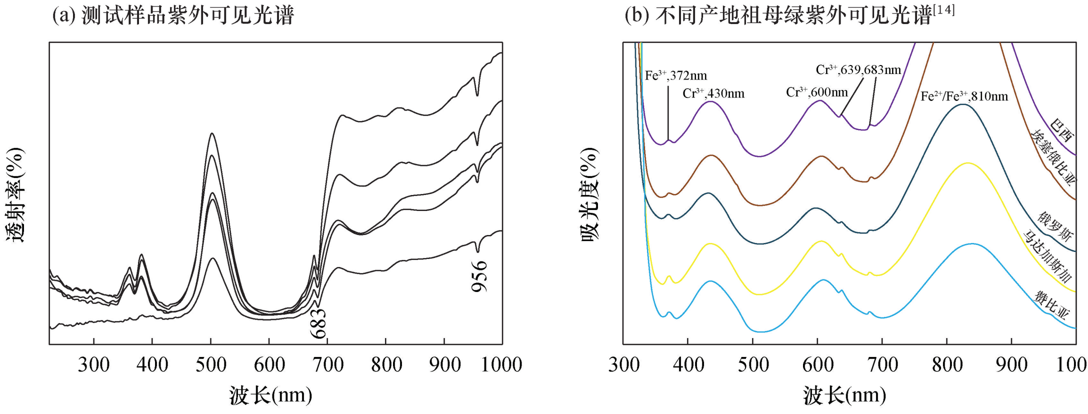

a—测试样品紫外可见光谱; b—不同产地祖母绿紫外可见光谱[14]。

图 3 测试样品和天然祖母绿的紫外可见光谱

Fig. 3 UV-visible spectra of the tested samples and natural emeralds. (a) UV-Vis spectra of tested samples; (b) UV-Vis spectra of emeralds from different origins[14].

过测试样品中 Ni 元素峰强度远高于 Cr 元素，这不符合天然祖母绿的元素含量特征，而与卢磊等[23]、杨燕菱等[24]报道的水热法合成祖母绿的 Ni 含量高的特征相吻合，说明测试样品为合成祖母绿。

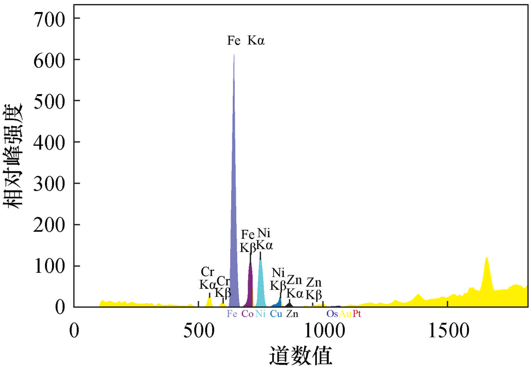

图 4　样品的能量色散型 X 射线荧光光谱图

Fig. 4　EDXRF of the samples.

4　水热法合成的各类祖母绿光谱特征分析

目前水热法合成祖母绿的公司较多，主要有：俄罗斯水热法合成祖母绿、Linde 合成祖母绿、Biron 合成祖母绿、Lechleitner 合成祖母绿、中国桂林水热法合成祖母绿等。石国华[1]分析了 Linde 合成祖母绿、俄罗斯水热法合成祖母绿、中国桂林水热法合成祖母绿的特征，前人研究结果认为“水波纹”状生长纹理及与 Cl^- 有关的红外吸收峰 2300～3100cm^{-1} 是其鉴定的重要特征。本文所测试样品无法通过红外吸收光谱、紫外可见光谱来确定，说明传统的鉴定手段对某些合成祖母绿的鉴定存在局限性。

Wood 等[12]、Qin 等[13]、Saeseaw 等[14]、Guo 等[15]、Krzemnicki 等[16]、Bai 等[17]研究了世界各个产地的祖母绿紫外可见吸收光谱特征，其中重要的一点是认为 Fe^{2+} 所致的吸收带 810～850nm 对于鉴定起到关键作用，只有极少数天然祖母绿这一吸收谱带特征不明显。本文所测试的样品这一吸收谱带均不明显，因此认为紫外可见光谱分析结果不能确定样品是否为天然祖母绿，但应引起质检人员的警示。

杨卓[2]、Karampelas 等[6]、Qin 等[13]、Bai 等[17]、Pignatelli 等[19]、Lum 等[20]分析了巴西、哥伦比亚、埃及、印度、南非、津巴布韦、加拿大、中国等不同产地祖母绿中的主量和微量元素特征，天然祖母绿中几乎不含 Ni 元素或含量极低，但均明显含有 Cr 元素，可见 Ni 元素含量远低于 Cr 元素含量，而本文所测试样品 Ni 的峰强度远高于 Cr 峰，这不符合天然祖母绿的元素含量特征。

5　结论

本文测试样品的红外吸收光谱特征与天然祖母绿相似，红外吸收光谱不能作为鉴定祖母绿成因的依据。前人研究结果表明红外吸收光谱中 2300～3100cm^{-1} 范围的一组吸收峰是水热法合成祖母绿的重要鉴定特征，但对于本文测试样品这一特征不明显。同时测试样品的紫外可见光谱显示与 Fe^{2+} 相关的 810～850nm 附近吸收带不明显，天然祖母绿几乎不含 Ni 元素，测试样品的 X 射线荧光光谱显示 Ni 元素峰强度远高于 Cr 元素是该类水热法合成的新型祖母绿的主要特征。由本文实验结果可见，珠宝玉石鉴定是一项系统工作，需要借鉴前人成果，结合多种检测方法的综合分析才能得到正确的结论。

水热法合成祖母绿的工艺复杂多变，随着技术的不断更新，质检机构应针对新出现的水热法合成祖母绿，注重宝石学和光谱学的综合分析。

Gemological and Spectral Characteristics of a New Type of Emerald Synthesized by the Hydrothermal Method

ZHU Hongwei[1,2], *CHENG Youfa*[1,2], *LI Ting*[1,2], *MA Xiao*[1,2], *DING Xiuyun*[1,2], *FAN Chunli*[1,2], *ZHAO Xiaoxue*[1,2], *CHEN Shuxiang*[3], *HU Jianhua*[4]

(1. Shandong Institute of Metrology, Jinan 250014, China;
2. National Gold & Diamond Testing Center, Jinan 250014, China;
3. Qilu University of Technology (Shandong Academy of Sciences), Jinan 250353, China;
4. Shenzhen Shenzhi Testing Technology Co., Shenzhen 518020, China)

HIGHLIGHTS

(1) Conventional gemological instruments and infrared spectroscopic analysis cannot determine the genesis of the new type of synthetic emeralds.

(2) The key detection features of this new type synthetic emerald are that the intensity of the Ni peak is much stronger than that of the Cr peak in EDXRF analysis and it is not obvious in the absorption band of 810-850nm in the UV-Vis spectroscopy.

(3) Accurate identification of this new type of synthetic emerald requires a comprehensive analysis by multiple methods.

ABSTRACT

BACKGROUND: The emerald is loved by people because of its gorgeous color and is respected as one of the world's four major gems. Due to the high value of emeralds, a variety of synthesis and optimization methods have emerged. The hydrothermal method is one of the common methods to produce synthetic emeralds. The emeralds synthesized by this method have typical water ripple texture, showing a serrated parallel arrangement, and the characteristic peaks of the infrared absorption spectrum in the range of 2300-3100cm^{-1} are the main identification feature. However, some emeralds synthesized by this method do not have the above typical characteristics. This has brought a great challenge to the quality inspection agencies, and brought many doubts to the majority of consumers, and affected the stability of the gem market.

OBJECTIVES: It is essential to study the new emerald synthesized by this new hydrothermal method. The refractive index, density, polychromatism, and infrared absorption spectrum characteristics of the tested samples are very similar to those of natural emeralds, so infrared absorption spectrum analysis cannot obtain the supporting evidence of its cause. Based on this, the gemological and spectral characteristics of the test samples were studied by ultraviolet visible spectrum, energy dispersive X-ray fluorescence spectrometry (EDXRF) and other spectroscopic means. Finally, the test samples were determined to be a new kind of emerald synthesized by the hydrothermal method.

METHODS: The refractive index, birefringence, relative density, polychromaticity and weight of the samples were tested by refractometer, electronic balance, and dichroic mirror. The internal and external characteristics of the test samples, the cutting and polishing quality of the samples, and the characteristics of internal inclusions were observed by gem microscope. The infrared reflection spectrum and infrared transmission spectrum characteristics of the samples were analyzed by Fourier transform infrared spectrometer and compared with the infrared spectrum characteristics of emeralds from different origins. The absorption spectrum characteristics of the samples were analyzed by ultraviolet-visible spectrometer, focusing on the absorption peak characteristics near 830nm. The element characteristics of the samples were tested by EDXRF, because the content characteristics of Cr and Ni in emerald are the key to identify whether it is natural or not.

RESULTS: The mass of the tested samples was 0.17-0.56g, the refractive index was 1.571-1.588, the birefringence was 0.007-0.009, the relative density was 2.56-2.78, and the polychromaticity was obviously blue-green/green. These conventional gemological characteristics were consistent with natural emeralds. The samples were observed under a gemstone microscope, and the samples had a parallel texture of suspected water ripple, but not typical. The water ripple texture of the typical hydrothermal synthetic emeralds was serrated parallel arrangement. However, the characteristics under the gem microscope should arouse the suspicion of jewelry inspectors.

The infrared reflectance spectra of the samples had characteristic peaks of 1242, 1219, 1022, 968, 810, 741, 687, 594, 528, 490, and 459cm^{-1}. The characteristic peaks of 1242, 1219, 1022, 968, 810, 741, and 687cm^{-1} were caused by the stretching vibration of Si—O—Si and O—Si—O, and the characteristic peaks of 594,

528, 490, and 459cm^{-1} were caused by the bending vibration of Si—O and the vibration of M—O. The infrared reflection spectrum characteristics of the samples were consistent with the infrared spectrum characteristics of beryl, but the infrared spectrum characteristics of the fingerprint area could not indicate whether the samples were natural or synthetic.

The infrared transmission spectra of the samples had 5445, 5273, 5109, 4874, 4800, 4650, 4547, 3321, 3222, 3027, 2953, 2928, and 2431cm^{-1} characteristic peaks. 5273cm^{-1} was caused by type Ⅱ water absorption, 5445cm^{-1} and 5109cm^{-1} were caused by type Ⅰ water absorption. The type Ⅱ water absorption peak of the test samples was relatively sharp at 5273cm^{-1}, and the type Ⅰ water absorption peaks at 5445cm^{-1} and 5109cm^{-1} were relatively strong. Compared with previous studies, the shape and intensity of water absorption peaks of natural emerald and hydrothermally synthesized emerald were different. The infrared absorption spectrum characteristics of the water of the test sample were different from those of natural emerald, but the diagnostic direct evidence could not be obtained from the infrared absorption spectrum. The infrared peak in the range of 2300-3100cm^{-1} is caused by Cl^- ion absorption. According to the results of previous studies, the absorption intensity of hydrothermal synthetic emeralds in this wavenumber range was significantly stronger than that of natural emeralds. The infrared absorption spectra of the test samples were relatively weak in the range of 2300-3100cm^{-1}, which was more similar to the infrared absorption spectrum characteristics of natural emeralds in Colombia, Yunnan, Madagascar and Brazil, and was obviously different from the infrared absorption spectrum results of emeralds synthesized by the hydrothermal method. There were obvious differences between the infrared transmission absorption spectra of the traditional hydrothermal synthetic emeralds and natural emeralds. The characteristics of infrared absorption spectra are important evidence for identifying the genesis of emeralds. However, it is difficult to obtain the final accurate conclusion from the infrared absorption spectrum analysis of the test samples described in this paper, so they have been named ‘new’ type.

The UV-Visible spectrum characteristics of the test samples showed that the absorption peak below 350nm was caused by the Fe^{2+}-O^{2-} charge transfer band in emerald, the absorption peak at 429nm was caused by Cr^{3+} ions, the broad absorption band at 550-650nm was mainly caused by Cr^{3+} ions, the absorption peak at 683nm was caused by Cr^{3+} ions, the sharp absorption peak at 956nm was caused by water absorption, and the broad absorption peak near 850nm should be caused by Fe^{2+} absorption, which was rarely seen in the previous hydrothermal synthesis of emerald. The combination of Cr^{3+} and Fe^{3+} replacing Al^{3+} makes emerald, green. The absorption peak of UV-Visible spectrum caused by Fe^{2+} in natural emerald was in the range of 810-850nm, and only a few of the absorption bands caused by Fe^{2+} in natural emeralds are not obvious. The absorption band of the UV-Visible spectra of the test samples was not obvious or weak in the range of 810-850nm, and the 850nm absorption peak of individual samples was obvious. Therefore, the emeralds examined by ultraviolet-visible spectroscopy may be synthetic, but this could not be conclusively confirmed.

The EDXRF results showed that the samples had Fe, Ni and Cr elements, which was different from previous studies of natural emeralds. Yang Zhuo (2010) studies showed that the main trace elements in natural emeralds, from different origins such as Brazil, Colombia, Egypt, India, South Africa, Zimbabwe and Canada by LA-ICP-MS, were Fe, V, Cr, Mg, Na and Cs, but the content of Ni was very low, far lower than that of Cr. The content of Cr in Yunnan emeralds was 58-177μg/g, and Ni was not detected (Bai et al., 2019). The chemical element characteristics of gem-grade emeralds in Afghanistan, Brazil, Colombia, Ethiopia, Madagascar, Russia, Zambia and Zimbabwe showed that Ni element was not detected (Karampelas et al., 2019). The elemental composition of emeralds from South Africa, Afghanistan, Australia, Colombia, Egypt, Madagascar, Zambia, Zimbabwe, Tanzania and China was analyzed by electron probe microanalysis, and Ni was not detected (Lum et al., 2016). It could be seen that Cr and Fe elements coexisted in natural emeralds, but Ni was almost non-existent. EDXRF was used in this study without quantitative analysis but calibrated by the gold standard sample, and the relative peak intensity of

the element was of great significance. The peak intensity of the Ni element in the test sample was much higher than that of the Cr element, which did not conform to the element content characteristics of the natural emerald, and was consistent with the high content of Ni in the hydrothermal synthesis of emerald reported by Lu and Shen (2021) and Yang et al. (2022). The comprehensive analysis showed that the test sample was a synthetic emerald.

CONCLUSIONS: The infrared absorption spectrum characteristics of the test samples are similar to those of natural emeralds, and the infrared absorption spectrum could not be used as a basis for identifying the genesis of emeralds. Previous studies show that a set of absorption peaks in the range of 2300－3100cm^{-1} in the infrared absorption spectrum is an important identification feature of the hydrothermal synthesis of emeralds, but this feature is not obvious in the tested samples. The UV-Visible spectrum of the sample shows that the absorption band near 810－850nm related to Fe^{2+} is not obvious. The X-ray fluorescence spectra of the samples show that the Kα peak intensity of Ni is much higher than that Kα of Cr, which is the main feature of the new emerald synthesized by the hydrothermal method. It could be seen from the experimental results that the identification of jewelry and jade is a systematic work. It is necessary to learn from the previous results and combine the comprehensive analysis of various detection methods to obtain the correct result.

KEY WORDS: emeralds; hydrothermal method; infrared spectroscopy; UV－Vis spectroscopy; X－ray fluorescence spectrometry; identification characteristics

参考文献

[1] 石国华. 桂林水热法合成祖母绿红外光谱特性及其意义[J]. 宝石和宝石学杂志,1999,1(1):40-44.
Shi G H. FTIR features of Guilin hydrothermally-grown synthetic emerald and its significance[J]. Journal of Gems and Gemmology,1999,1(1):40-44.

[2] 杨卓. 云南和其他地区祖母绿产地特征的对比研究[D]. 北京:中国地质大学(北京),2010.
Yang Z. Comparative study on locality features of emerald in Yunnan and which in other areas of the world[D]. Beijing:China University of Geosciences (Beijing),2010.

[3] 孙主,李娅丽. 俄罗斯水热法合成祖母绿的宝石学特征研究[J]. 宝石和宝石学杂志,2010,12(1):12-15.
Sun Z, Li Y L. Study on gemological characteristics of Russian hydrothermal synthetic emerald[J]. Journal of Gems and Gemology,2010,12(1):12-15.

[4] 申柯娅. 天然祖母绿与合成祖母绿的成分及红外吸收光谱研究[J]. 岩矿测试,2011,30(2):233-237.
Shen K Y. Study on chemical compositions and infrared absorption spectra of natural and synthetic emeralds[J]. Rock and Mineral Analysis,2011,30(2):233-237.

[5] 邵慧娟,亓利剑,钟倩,等. 俄罗斯富铁型水热法合成祖母绿特征研究[J]. 宝石和宝石学杂志,2014,16(1):26-34.
Shao H J,Qi L J,Zhong Q,et al. Study on characteristics of iron-rich hydrothermal synthetic emerald from Russia,2014,16(1):26-34.

[6] Karampelas S,Al-Shaybani B,Mohamed F,et al. Emeralds from the most important occurrences:Chemical and spectroscopic data[J]. Minerals,2019,9:561-590.

[7] Huong L T,Hofmeister W,Häger T,et al. A preliminary study on the separation of natural and synthetic emeralds using vibrational spectroscopy[J]. Gems & Gemology,2014,50(4):287-292.

[8] 吴瑾光. 近代傅里叶变换红外光谱技术及应用[M]. 北京:科学技术文献出版社,1994.
Wu J G. Modern Fourier transform infrared spectroscopy and its application[M]. Beijing:Science and Technology Literature Press,1994.

[9] 彭文世,刘高魁. 矿物红外光谱图集[M]. 北京:科学出版社,1982.
Peng W S,Liu G K. Atlas of mineral infrared spectroscopy[M]. Beijing:Science Press,1982.

[10] 张嘉麟,张倩,裴景成,等. 水热法合成蓝绿色绿柱石的宝石学及光谱学特征[J]. 光谱学与光谱分析,2021,41(7):2258-2262.
Zhang J L,Zhang Q,Pei J C,et al. Gemological and spectroscopy characteristics of synthetic blue-green beryl by hydrothermal method[J]. Spectroscopy and Spectral Analysis,2021,41(7):2258-2262.

[11] 张蓓莉. 系统宝石学[M]. 北京:地质出版社,2006.
Zhang B L. Systematic gemology[M]. Beijing:Geology Press,2006.

[12] Wood D L,Nassau K. The characterization of beryl and emerald by visible and infrared absorption spectroscopy[J]. American Mineralogist,1968,53(5-6):777-800.

[13] Qin L J, Yu X Y, Guo H S. Fluid inclusion and chemical composition characteristics of emeralds from Rajasthan area, India[J]. Minerals, 2022, 12: 1-20.

[14] Saeseaw S, Nathan D R, Aaron C P, et al. Geographic origin determination of emerald[J]. Gems & Gemology, 2019, 55(4): 614-646.

[15] Guo H S, Yu X Y, Zheng Y Y, et al. Inclusion and trace element characteristics of emeralds from Swat Valley, Pakistan[J]. Gems & Gemology, 2020, 56(3): 336-355.

[16] Krzemnicki M S, Wang H A O, Büche S. A new type of emerald from Afghanistans Panjshir Valley [J]. The Journal of Gemology, 2021, 37(5): 474-495.

[17] Bai F, Pan H H, Li X M. Replacement degree of Al^{3+} and Cr/V ratio in high-V emeralds from Malipo, Yunnan, China [J]. Arabian Journal of Geosciences, 2019, 12: 376-385.

[18] 乔鑫, 周征宇, 农佩臻, 等. 贫碱结构水类型祖母绿红外光谱特征及其控制因素探究[J]. 岩矿测试, 2019, 38(2): 169-178.

Qiao X, Zhou Z Y, Nong P Z, et al. Study on the infrared spectral characteristics of H_2O Ⅰ-type emerald and the controlling factors [J]. Rock and Mineral Analysis, 2019, 38(2): 169-178.

[19] Pignatelli I, Giuliani G, Ohnenstetter D. Colombian trapiche emeralds: Recent advances in understanding their formation[J]. Gems & Gemology, 2015, 51(3): 222-259.

[20] Lum J E, Viljoen K S, Cairncross B. Mineralogical and geochemical characteristics of emeralds from the Leydsdorp area, South African[J]. South African Journal of Geology, 2016, 119(2): 359-378.

[21] 任伟, 汪立今, 李甲平. 电子探针和 X 射线衍射仪测定新疆祖母绿宝石[J]. 岩矿测试, 2010, 29(2): 179-181.

Ren W, Wang L J, Li J P. Detection of emerald from Xinjiang by electron probe microanalyzer and X-ray diffractometer[J]. Rock and Mineral Analysis, 2010, 29(2): 179-181.

[22] 代鸿章, 王登红, 刘丽君, 等. 电子探针和微区 X 射线衍射研究陕西镇安钨-铍多金属矿床中祖母绿级绿柱石[J]. 岩矿测试, 2018, 37(3): 336-345.

Dai H Z, Wang D H, Liu L J, et al. Study on emerald-level beryl from the Zhen'an W-Be polymetallic deposit in Shaanxi Province by electron probe microanalyzer and micro X-ray diffractometer [J]. Rock and Mineral Analysis, 2018, 37(3): 336-345.

[23] 卢磊, 沈锡田. 市场上"重结晶祖母绿"的鉴定特征[J]. 宝石和宝石学杂志, 2021, 3(5): 51-59.

Lu L, Shen X T. Identification characteristics of "recrystallized synthetic emerald"[J]. Journal of Gems and Gemology, 2021, 3(5): 51-59.

[24] 杨燕菱, 沈锡田, 范玉蓉, 等. 俄罗斯富钒型水热法合成祖母绿的紫外-可见-近红外光谱表征[J]. 光谱学与光谱分析, 2022, 42(4): 1199-1203.

Yang Y L, Shen X T, Fan Y R, et al. UV-Vis-NIR spectroscopic characteristics of vanadium-rich hydrothermal synthetic emeralds from Russia [J]. Spectroscopy and Spectral Analysis, 2022, 42(4): 1199-1203.